Equatorial Pacific Ocean Horizontal Velocity, Divergence, and Upwelling*

G REGORY C. J OHNSON AND M ICHAEL J. M C P HADEN

NOAA/Pacific Marine Environmental Laboratory, Seattle, Washington

E RIC F IRING

Department of Oceanography, University of Hawaii, Honolulu, Hawaii

ABSTRACT

Upper-ocean horizontal velocity and divergence were estimated from shipboard observations taken from 1991 to 1999 in the equatorial Pacific between 170°W and 95°W. Mean transports were estimated for the zonal currents at the mean longitude of the sections, 136°W. Mean meridional currents for the entire longitude range included poleward surface flows reaching -0.09 m s^{-1} in the south and 0.13 m s^{-1} in the north as well as equatorward flow within the thermocline reaching 0.05 m s^{-1} in the south and -0.04 m s^{-1} in the north near 23°C (85 m). Vertical velocity was diagnosed by integrating horizontal divergence estimated for the entire region down from the surface. Equatorial upwelling velocities peaked at 1.9 (± 0.9) $\times 10^{-5}$ m s^{-1} at 50 m. The upwelling transport in the area bounded by 3.6°S–5.2°N, 170°W–95°W was 62 (± 18) $\times 10^{6}$ m^3 s^{-1} at 50 m. Strong downwelling was apparent within the North Equatorial Countercurrent. An asymmetry in the meridional flows suggested that on the order of 10×10^6 m^3 s^{-1} of thermocline water from the Southern Hemisphere was upwelled at the equator and moved into the Northern Hemisphere as surface water. This interhemispheric exchange path could be part of the route for water from the Southern Hemisphere to supply the Indonesian Throughflow.

1. Introduction

The general circulation of the equatorial Pacific Ocean is characterized by strong wind-driven zonal flows and a complex meridional circulation involving shallow overturning cells (Lu et al. 1998). There is a long history of describing and analyzing the intense zonal currents, both their means (e.g., Wyrtki and Kilonsky 1984, hereafter WK) and their spatiotemporal variability (e.g., Taft and Kessler 1991). The weaker meridional circulation and upwelling within a few degrees of the equator (e.g., Wyrtki 1981) are not only important elements of the general circulation, but they also exert a strong control on global climate and biogeochemical cycles (e.g., Philander 1990; Chavez et al. 1999). However, being weaker, these elements of the circulation are subject to aliasing over a wide variety of time and space scales, and are much more difficult to observe than the zonal currents.

---

* Pacific Marine Environmental Laboratory Contribution Number 2181.

Corresponding author address: Dr. Gregory C. Johnson, NOAA/ Pacific Marine Environmental Laboratory, 7600 Sand Point Way N.E., Bldg. 3, Seattle, WA 98115-0070.
E-mail: gjohnson@pmel.noaa.gov

Equatorial upwelling likely has a magnitude of a meter per day ($\sim 1 \times 10^{-5}$ m s^{-1}). While this value is large compared with most of the rest of the ocean, it is still much too small to measure directly. This inability to make direct measurements of upwelling has significant consequences. For example, in equatorial upper-ocean heat budgets, terms related to upwelling and vertical mixing must be estimated as residuals. These residuals can be as large as or larger than any of the other terms in the budget (cf. Wang and McPhaden 1999).

As a result, equatorial upwelling has been estimated in a number of ways over a number of spatial and temporal scales. Weisberg and Qiao (2000, hereafter WQ) provide a recent review. In the Pacific Ocean chemical tracers have been used with mixing models to estimate upwelling transports (Quay et al. 1983) and to deduce upwelling sources (Fine et al. 1983). Large-scale calculations assuming Ekman and geostrophic dynamics have been made to diagnose upwelling (Wyrtki 1981; Bryden and Brady 1985). Surface drifter velocities have been used to estimate meridional divergence and infer upwelling (Poulain 1993). Local direct estimates of horizontal divergence from moored current meter arrays have been integrated vertically to estimate vertical velocity on the equator by continuity (Halpern et al. 1989; WQ). A similar approach has also been applied over larger scales using 27 repeat shipboard acoustic Doppler
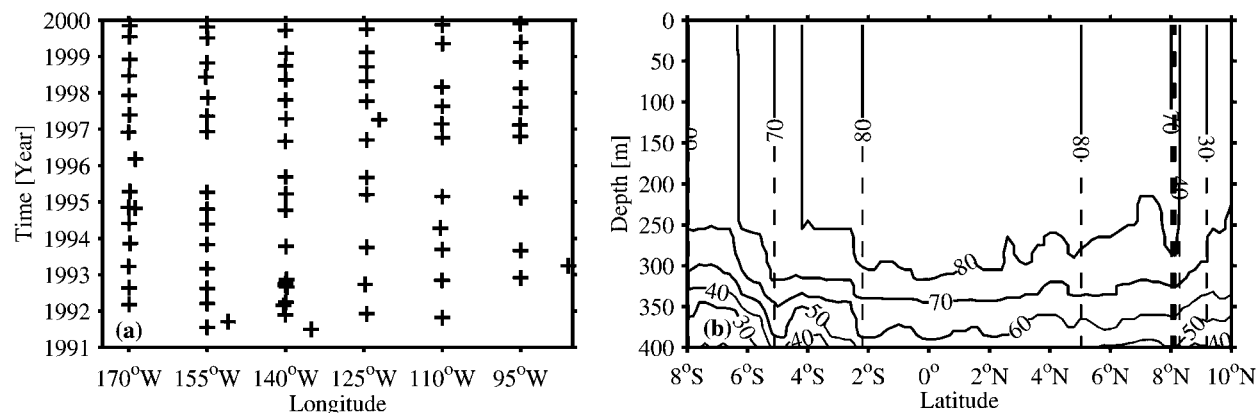
FIG. 1. Data distribution: (a) CTD/ADCP section longitudes and times; each plus represents a section. (b) Number of sections occupying each latitude and depth for ADCP velocities (solid contours) and CTD temperature and salinity (dashed contours); contour intervals 10.

current profiler (ADCP) sections from the Hawaii-to-Tahiti Shuttle experiment (Johnson and Luther 1994). These data also gave direct observations of the off-equatorial meridional velocity field and allowed off-equatorial vertical velocity estimates.

Here shipboard conductivity–temperature–depth (CTD) and ADCP data from 85 meridional sections taken across the equator from 1991 to 1999 between 170°W and 95°W were used to make meridionally localized estimates of the zonal flow, and large-scale estimates of the meridional flow and horizontal divergence in the upper tropical Pacific Ocean. This work closely followed that of Johnson and Luther (1994). However, an independent dataset was used with three times the number of ADCP sections, much lower instrument error, and greater latitude, longitude, and depth ranges. The results were more certain estimates over a larger area. Upwelling was calculated from continuity to generate an upper-ocean meridional–vertical section of vertical velocity for the region. Section 2 describes the data and how the fields and their errors were estimated. Section 3 discusses zonal velocity, temperature, salinity, and zonal currents, all estimated locally near the central longitude of the domain. Section 4 discusses meridional velocity, both components of the large-scale horizontal divergence, and the vertical velocity field (hence the upwelling transport) inferred from integration of this divergence. Section 5 concludes the paper by discussing the results and comparing them to previous work.

2. Data, methods, and errors

The 85 meridional CTD/ADCP sections used were taken from June 1991 through December 1999 (Fig. 1a). Of these sections, 73 were taken during Tropical Atmosphere–Ocean (TAO) buoy array maintenance cruises. The TAO cruises were on the NOAA Ship *Discoverer* in the first half of the decade (Johnson and Plimpton 1999) and the NOAA Ships *Ka'imimoana* and *Ronald H. Brown* for the second half of the decade. A subset

of these sections has been used to study the 1997–98 El Niño (Johnson et al. 2000). Another seven sections were from World Ocean Circulation Experiment one-time hydrographic survey cruises on several different ships. The remaining five sections were from U.S. Joint Global Ocean Flux Study Equatorial Pacific Process Study (Murray et al. 1995) cruises on the R/V *Thomas G. Thompson*.

The individual ADCP and CTD sections were gridded following Johnson et al. (2000). The ADCP velocities were objectively mapped assuming a Gaussian covariance, meridional correlation length scales of 1°, vertical correlation length scales of 25 m, and a noise-to-signal energy ratio of 0.01. The CTD temperature, salinity, and pressure data were splined in latitude on isopycnals. These gridded sections were used in all subsequent analysis.

TAO cruises occupied meridional sections nominally from 8°S to 8°N at 15° longitude intervals between 170°W and 95°W. At 140°W the nominal latitude range was from 5°S to 9°N. Two adjacent sections were often occupied during a single cruise, one steaming southward across the equator and another steaming northward across the equator at least a week later. The resulting 7-day temporal and 1660-km spatial separation were assumed sufficient for each section to be independent, at least in terms of the energetic high-frequency ocean variability (including internal waves, equatorial Kelvin waves, Rossby waves, and tropical instability waves) in the region. This assumption probably holds best for the meridional velocity data, where a very small mean signal is often overwhelmed by large transients such as tropical instability waves (Flament et al. 1996). However, even for zonal velocity these separations would be sufficient to sample different phases of an equatorial Kelvin wave (if the eastern section of the pair were occupied first). The data did not always span the entire latitude and depth range studied (Fig. 1b), with less CTD and ADCP data off the equator and less ADCP data below 250 m.

Instrumental errors were thought to be negligible compared with the ocean variability mentioned above. The CTD accuracies were near 1% for pressure, 0.002°C for temperature, and 0.003 PSS-78 for salinity. Velocity accuracies for the ADCP were near 0.05 m s^{-1}. These errors would have been mostly in the cross-track component (the zonal velocity for these meridional sections), and generally not systematic over an entire section. These quasi-random errors were assumed very unlikely to lead to systematic errors in currents or their divergences when averaged over the large number of cruises and sections involved.

The spatiotemporal distribution of sections (Fig. 1a) had some biases. From 11 to 13 sections were occupied in each of the years 1992 and 1997–99, with 6–9 sections in each of the other 4.5 years. For June 1991–December 1999 the monthly Southern Oscillation index (SOI) mean and standard deviation were -0.5 ± 0.9, slightly favoring El Niño conditions. The same statistics held for the SOI interpolated to section times. The sampling favored the western longitudes. The mean longitude of the sections, 136°W, was slightly west of the central longitude of the domain, 132°W. Finally, the sampling was somewhat biased toward boreal spring and especially biased toward boreal fall. The most uneven 3-month groupings included only 13 sections in December–February and 11 in June–August, but 22 in March–May and 39 in September–November.

The effects of these sampling biases were explored in the context of the zonal wind stress. The Florida State University surface wind analyses (Stricherz et al. 1992) were interpolated to section locations and times. From 8°S to 10°N, generally under the easterly trade winds over the longitude range in question, the zonal means of the section-interpolated zonal wind stresses were roughly 0.9 times the 1961–90 zonal means over the entire longitude range. It seems that the effects of sampling favoring El Niño, which should tend to decrease the trade winds, slightly more than counterbalanced the sampling favoring the boreal fall and the west, which should tend to increase the trade winds. Weaker trade winds would generally tend to reduce the strength of the South Equatorial Current (SEC) and Equatorial Undercurrent (EUC), as well as the surface Ekman divergence, thermocline geostrophic convergence, and upwelling.

Estimates of zonal velocity, u; temperature, T; and salinity, S, were made at the mean longitude of the sections, 136°W. To make these estimates data from all sections were fit to a third-order polynomial function of longitude at each latitude and depth. This procedure smoothed the fields, while still allowing sufficient degrees of freedom to model features such as the EUC maximum in the center of the region, the eastward shoaling of the thermocline, and the like. Additions of an annual harmonic and/or linear SOI response to the regression were tested, but were left out to avoid introducing noise into the means. For the most part, these fits were only used near the center of the region, where they were best determined.

Estimates of meridional velocity v, both components of horizontal divergence, and vertical velocity w were made only for the entire region encompassed by the sections. This strategy was necessitated by the fact that the small mean v was highly aliased by very energetic transient features. In fact, v was so noisy that attempts to regress against various combinations of longitude, the annual cycle, and the SOI (with the possible exception of the last) were all judged to have simply introduced noise into the resulting mean field. Thus, v and its meridional derivative, v_y, had to be estimated disregarding the longitudinal and temporal variations anticipated in those fields. At each depth and latitude, all the v data within a 2° lat window were fit linearly versus latitude. These fits were evaluated at the centers of the window to determine v, and the fit slopes were used for v_y. The horizontal divergence is the sum of v_y and u_x, the zonal derivative of the zonal velocity. Since v_y had to be estimated uniformly over the entire longitude range, for consistency u_x was also estimated over the entire longitude range. Slopes of linear fits versus longitude to all the u data at each depth and latitude were used for u_x. This method gave results very similar to a difference of the mean zonal velocities at 95° and 170°W, but used all the data.

Near-surface velocity and divergence estimates merit a caveat. The shallowest data from the shipboard ADCP were at 20 m, but the gridded velocities were objectively mapped to 5 m. Velocities above 20 m were essentially linearly extrapolated by the mapping, mostly using vertical shear from 20 to 30 m, but with some influence from as deep as 50 m. Where the mixed layer was absent, or deep enough to exceed 30 m, the mapping likely produced reasonable results. However, where the thermocline was strong and the mixed layer was shallower than 30 m the extrapolation may have been problematic because of shear changes at the mixed layer base. Thus, the thermocline ridge around 10°N between the North Equatorial Countercurrent (NECC) and the North Equatorial Current was a suspect region.

A check on the ADCP velocities mapped to 15 m was allowed by velocities from drifter data between 150° and 130°W (Baturin and Niiler 1997). Both components of the mean mapped ADCP velocities at 15 m agreed (within standard errors) with the drifter means almost everywhere. The only (barely) significant difference was, as anticipated, near 10°N, where mean mapped ADCP velocities at 15 m showed a sharp reduction in northward velocity that was not so marked in the drifter means. Hence, the strength of downwelling in the NECC should be viewed skeptically.

A delete-one jackknife approach (Efron 1982) was used to estimate sampling errors, which were always reported here as standard errors of the mean. The procedure involved doing each calculation 85 times, omitting a section at a time to gain 85 slightly different
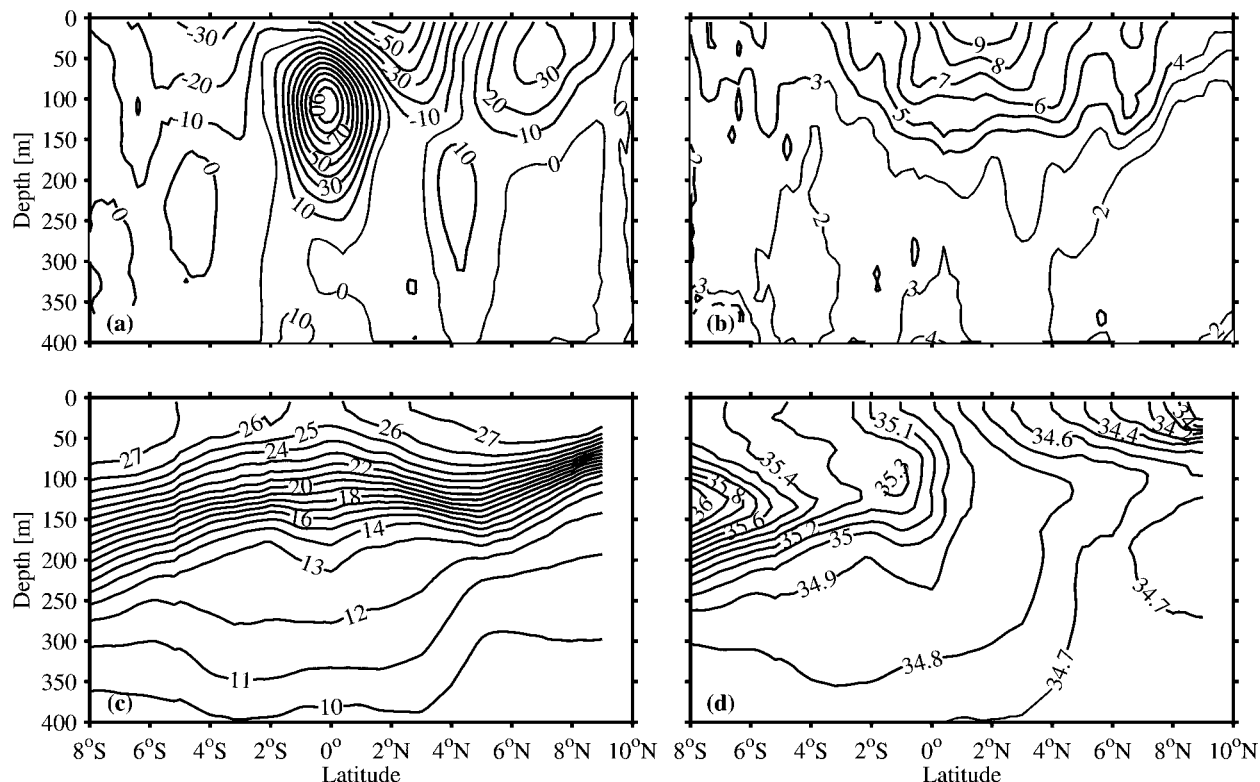
Fig. 2. Vertical–meridional sections at 136°W based on third-order polynomial fits vs longitude of data taken from 170° to 95°W (see text). (a) Zonal velocity u (10^{-2} m s^{-1}); contour intervals (CI) 10, positive (eastward) shaded. (b) Standard error of u, e_u (10^{-2} m s^{-1}); CI 1, $|u| > e_u$ shaded. (c) Temperature, T (°C); CI 1. (d) Salinity, S (PSS-78); CI 0.1.

estimates from which standard errors could be inferred. As already argued, each section was assumed to be independent and measurement errors were assumed to be negligible compared with sampling errors. For simple calculations like the uncertainty of an arithmetic mean, the jackknife estimate gives exactly the same answer for the standard error of the mean as one would obtain using more conventional methods. However, when doing operations like estimating the zonal velocity-weighted temperature of a current, the jackknife approach propagates the effects of spatial and temporal correlations by systematically removing contemporaneous u and T data for each calculation. The same advantage holds for more complex operations like computing the sums of u_x and v_y at every depth and latitude, and then integrating these sums vertically to infer w.

3. Zonal velocity, temperature, salinity, and transport

The meridional structure of the zonal velocity, temperature, and salinity are discussed in this section at the mean longitude of all sections used, 136°W, where estimates were the most reliable. The zonal structure of these fields along the equator is also discussed. Zonal current transports and associated properties are presented at 136°W. All of the fields discussed in this sec-

tion were estimated from third-order polynomial fits versus longitude using data from 170° to 95°W.

The u field at 136°W (Fig. 2a) clearly showed the major current structures. While some of the currents discussed were not delineated by the 0.1 m s^{-1} contour (Fig. 2a), they were discernible where their magnitudes exceed one standard error (shading in Fig. 2b). Eastward flowing currents included the NECC with a velocity maximum (core) at 7°N, 50 m; the EUC with a core at 0°, 110 m; and the Northern Subsurface Countercurrent (NSCC) with a core at 4°N, 210 m. The two very weak branches of the Southern Subsurface Countercurrent (SSCC) had cores at 4.5°S, 220 m and 7°S, 290 m (shading in Fig. 2b). Westward flowing currents included the northern branch of the SEC with a core at 2°N, 0 m; the southern branch of the SEC with a core at 4°S, 0 m; and the Equatorial Intermediate Current (EIC) with a core at 2.5°N, 330 m (shading in Fig. 2b). There was also significant eastward flow with a core at 1.5°S, 400 m, and westward flow with a core at 3.5°S, 330 m (shading in Fig. 2b). These flows were not analyzed because they appeared to extend beyond the 400-m depth range. The same held for all westward flow north of the NSCC and under the NECC because it appeared to extend beyond the 10°N latitude range.

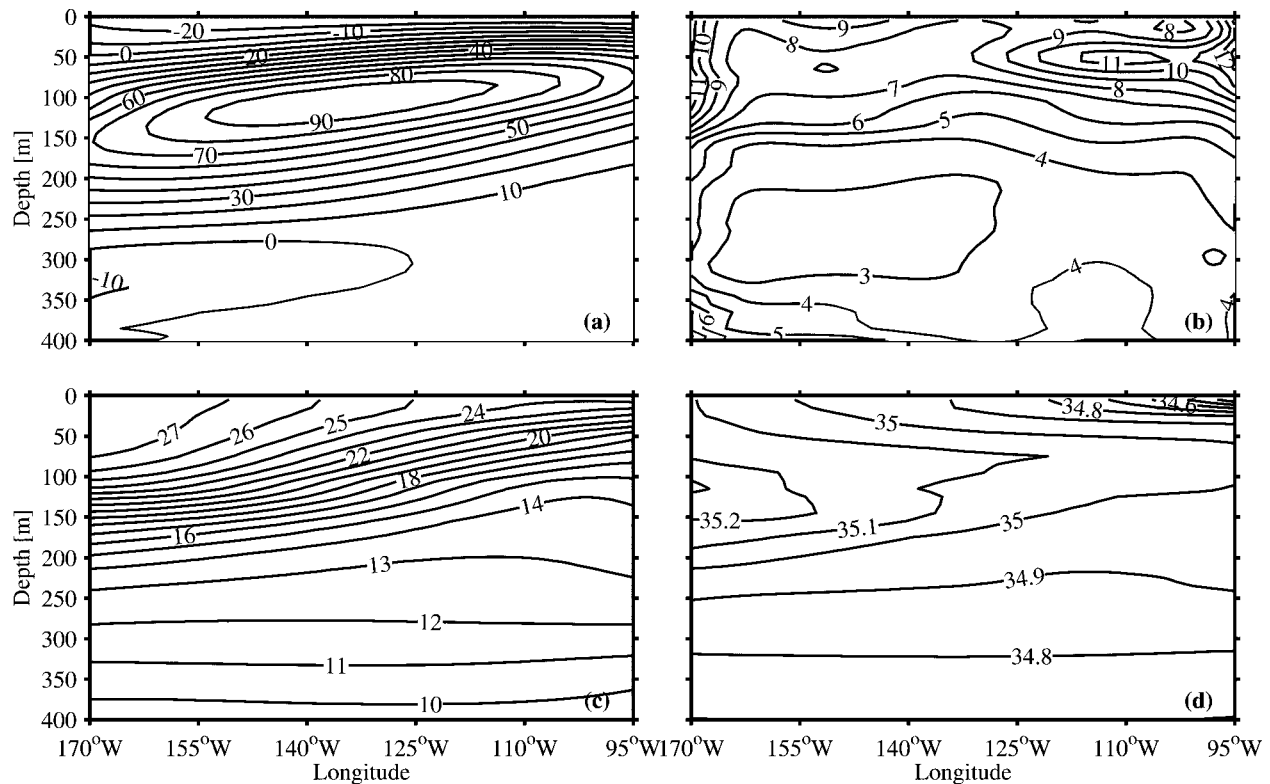The u field along the equator (Fig. 3a) was quite

FIG. 3. Vertical–zonal sections along the equator based on third-order polynomial fits vs longitude of data taken from 170° to 95°W (see text). Longitudes displayed denote nominal section locations. (a) Zonal velocity, u (10^{-2} m s^{-1}); contour intervals (CI) 10, positive (eastward) shaded. (b) Standard error of u, e_u (10^{-2} m s^{-1}); CI 1, $|u| > e_u$ shaded. (c) Temperature, T (°C); CI 1. (d) Salinity, S (PSS-78); CI 0.1.

similar to the mean zonal velocity from moored current meters on the equator (Yu and McPhaden 1999, their Fig. 2d). In fact, the u field along the equator agreed to within one standard error with means from moored TAO array ADCP data (Yu and McPhaden 1999) on the equator at three longitudes taken over a similar period, June 1991 through late 1999 (Fig. 4). The EUC shoaled from west to east, with zonal velocities peaking near the center of the region. Surface westward flow on the equator in the SEC was relatively constant across the domain. However, while the SEC on the equator reached nearly 50 m at 170°W it was limited to above the upper 20 m by 110°W. Below the EUC, westward flow of the EIC was found on the equator west of 125°W, strengthening to the west.

The standard errors of u (Fig. 2b) were surface and equatorially intensified but dropped to about 0.02 m s^{-1} outside of these regions. The peak of 0.10 m s^{-1} was centered near 1.5°N, 0 m. High variance extended across the EUC and northern branch of the SEC. A secondary maximum of 0.06 m s^{-1} was associated with the NECC near 7°N, 0 m. Along the equator (Fig. 3b) the standard errors of u were again mostly surface intensified. They also increased near the ends of the domain, as expected where the third-order fit was less well constrained. In addition, a subsurface maximum existed at 50 m from

125° to 95°W, associated with the upper part of the EUC in the thermocline (Fig. 3c).

The mean temperature and salinity fields were typical of the equatorial Pacific, and are shown mainly for reference to the other fields. The coolest surface water at 136°W was found on the equator (Fig. 2c), there was some spreading of the thermocline at the core of the EUC, a trough existed between the NECC and the northern branch of the SEC, and a deep thermostad was observed near 13°C between the SSCC and NSCC. Along the equator (Fig. 3c) the most prominent features were the shoaling of the thermocline and the strengthening of the 13°C thermostad to the east. Fresh surface water was observed to the north at 136°W under the intertropical convergence zone (Fig. 2d), salty water within the southern thermocline, a meridional salinity front at the equator within the thermocline where freshwater from the north and salty water from the south converged, a maximum just south of the equator associated with the EUC, and another weaker front below the thermocline associated with the NSCC (Johnson and McPhaden 1999). Along the equator (Fig. 3d), the salinity maximum associated with the EUC weakened to the east, under a fresh surface layer that strengthened to the east.

Direct estimates of cross-sectional areas, mean zonal velocities, volume transports, temperatures, and salini-
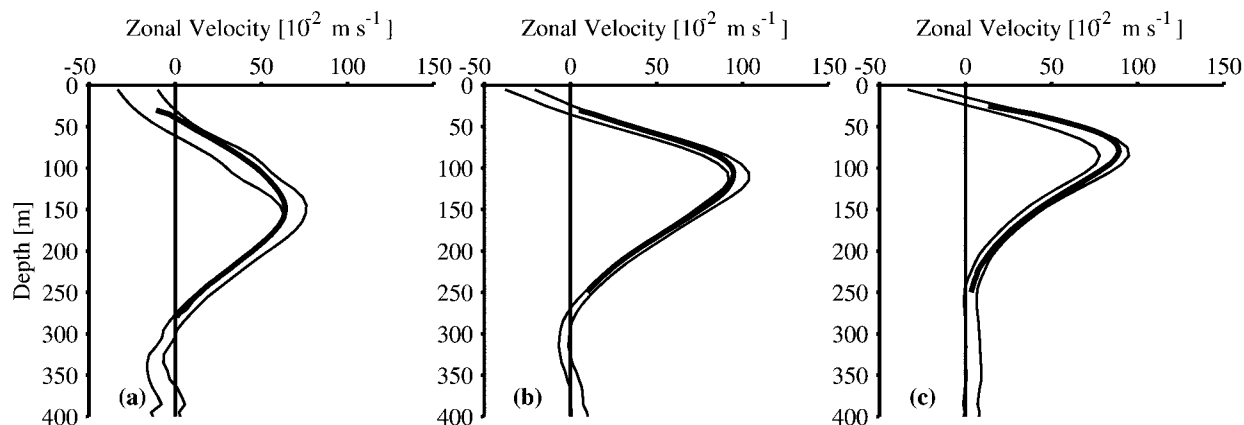
FIG. 4. Vertical profiles of equatorial zonal velocity, u (10^{-2} m s^{-1}) based on third-order polynomial fits vs longitude of data taken from 170° to 95°W (thin solid lines show one standard error about the mean, see text) compared to means of moored TAO ADCP records (thick lines dash–dot lines): (a) 170°W (moored data Jun 1991–Oct 1999), (b) 140°W (moored data Jun 1991–Aug 1995, and Sep 1996–Sep 1999), (c) 110°W (moored data Jun 1991–Nov 1999).

ties of these currents were made at 136°W (Table 1). Currents were defined as regions of unidirectional flow. There were three pairs of adjoining currents flowing in the same directions that required an additional definition to distinguish them: the NECC and NSCC, the EIC and the northern branch of the SEC, and the southern branch of the SEC and the deeper westward current centered near 3.5°S, 340 m. The boundaries between these three current pairs were defined by the velocity minima between them. The temperature and salinity means for each current are velocity weighted.

These estimates can be compared with earlier ones made between 158° and 150°W using hydrographic data from the 1979–80 Hawaii-to-Tahiti Shuttle (WK), roughly 2000 km to the west. While no error bars were given for the earlier estimates, there are many areas of agreement within the error bars given here. However, the NECC and south branch of the SEC reported here were weaker than the previous estimates, as might be expected with Sverdrup transports increasing westward. In addition, the eastward EUC reported here was stronger while the westward EIC was weaker than the pre-

vious estimates, consistent with the zonal structure of zonal velocity along the equator (Fig. 2a).

4. Meridional velocity, horizontal divergence, and vertical velocity

As noted before, noise in v set the strategy for its estimation as a function of depth and latitude only, without regard to longitude. The same held for v_y, which was estimated over a 2° lat window. To match the zonally independent estimate of v_y, u_x was estimated for the entire longitude range from the slopes of linear fits of all u data versus longitude at each depth and latitude. When these two quantities were summed to obtain the horizontal divergence and then integrated vertically, the resulting w field was estimated over the entire longitude range, meridionally smoothed over about 2° latitude.

At a sufficient distance from the equator, the v field (Fig. 5a) was presumably the sum of surface-intensified Ekman divergence due to the easterly trade winds and geostrophic convergence due to the eastward shoaling of the thermocline. The observations showed equatorial

TABLE 1. Mean zonal currents in the upper 400 m at 136°W. Estimates are based on third-order polynomial fits vs longitude of data from 85 meridional CTD/ADCP sections taken from 170° to 95°W during 1991–99 (see text). Temperatures and salinities are velocity weighted. Uncertainties are one standard error of the mean.

Current acronym	Area (10^6 m^2)	Speed (m s^{-1})	Transport (10^6 m^3 s^{-1})	Temperature (°C)	Salinity (PSS-78)
NECC	93 ± 7	0.15 ± 0.03	14 ± 2	24.4 ± 0.3	34.46 ± 0.03
SEC*	53 ± 6	−0.26 ± 0.06	−14 ± 3	25.5 ± 0.4	34.72 ± 0.03
SEC**	176 ± 10	−0.11 ± 0.01	−19 ± 2	23.3 ± 0.4	35.33 ± 0.03
EUC	101 ± 11	0.27 ± 0.03	28 ± 3	18.2 ± 0.4	35.07 ± 0.01
NSCC	61 ± 10	0.07 ± 0.02	4 ± 1	11.5 ± 0.1	34.74 ± 0.01
SSCC	42 ± 10	0.03 ± 0.01	1 ± 1	11.9 ± 0.4	34.87 ± 0.03
EIC	70 ± 11	−0.05 ± 0.02	−3 ± 2	11.4 ± 0.2	34.79 ± 0.01

* 0°–5°N
** 8°S–0°
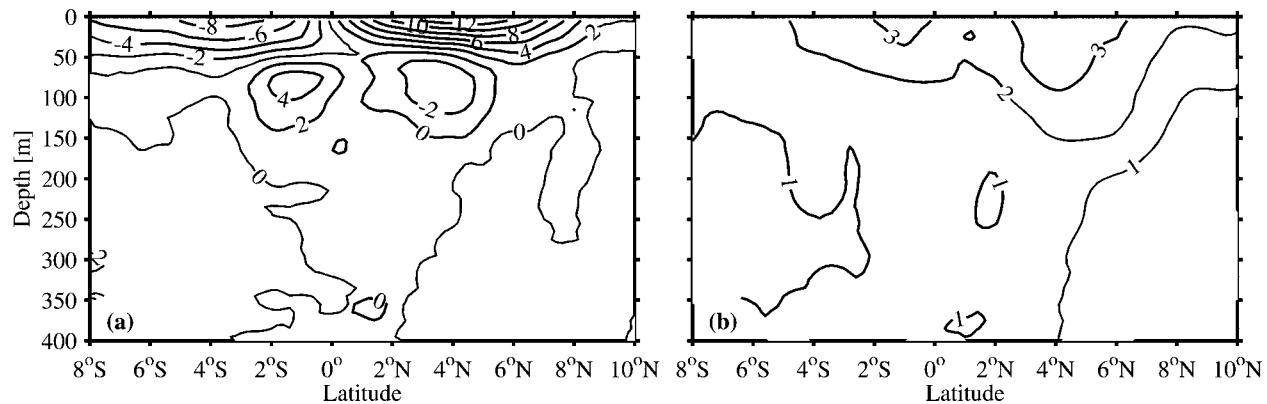
FIG. 5. Vertical–meridional sections based on centered 2° lat linear fits to data taken from 170° to 95°W, regardless of longitude (see text). (a) Meridional velocity, v (10^{-2} m s^{-1}); CI 2, positive (northward) shaded. (b) Standard error of v, e_v (10^{-2} m s^{-1}); CI 1, $|v| > e_v$ shaded.

surface divergence and thermocline convergence, and little cross-equatorial flow. Meridional velocities were much smaller than zonal velocities. Hence contour intervals for v were five times finer than for u. Poleward values of v were significant to 40–50 m (27°–25°C). Peak poleward surface speeds were -0.09 ± 0.02 m s^{-1} at 4.2°S and 0.13 ± 0.03 m s^{-1} at 4.6°N. Surface drifters also show stronger poleward flow in the north than in the south from 150° to 130°W (Baturin and Niiler 1997), despite the stronger trades in the Southern Hemisphere (Hellerman and Rosenstein 1983). Equatorward subsurface speeds were significant in the Southern Hemisphere from 60 m (24°C) through 160 m (15°C) and in the Northern Hemisphere from 60 m (25°C) through 110 m (21°C). Interior equatorward velocities peaked at 0.05 ± 0.02 m s^{-1} at 1.4°S and -0.04 ± 0.03 m s^{-1} at 3.6°N at 85 m (near 23°C).

Meridional geostrophic velocities estimated from vertical integrals of zonal density gradients (not shown) were generally equatorward over the entire latitude range. They were also surface intensified and stronger in the south. This hemispheric asymmetry was consistent with the direct measurements of equatorward transports. Since the equatorward geostrophic velocities were surface intensified, the wind-driven poleward Ekman component must have persisted to at least where the maximum in equatorward flow was observed, roughly 85 m. This penetration depth was well below the mixed layer depth (Figs. 2c and 2d).

The standard errors of v (Fig. 5b) were also surface intensified with off-equatorial maxima and dropped below 0.01 m s^{-1} in places. The maxima were 0.04 m s^{-1} at 4.5°N and 0.03 m s^{-1} at 1°S, and were likely related to tropical instability wave activity on both sides of the equator, but somewhat weaker in the south (Chelton et al. 2000). While the mean meridional currents were nearly an order of magnitude smaller than the mean zonal currents, the v standard errors were still half the magnitude of those for u. This combination of energetic transient variability and a weak mean resulted in a low

signal-to-noise ratio for v. In contrast to the u field, the v exceeded their standard errors (shading in Fig. 5b) mainly near the surface and in the thermocline on either side of the equator.

Since seawater is nearly incompressible and vertical velocity, w, is negligible at the surface, the horizontal divergence, $u_x + v_y$, can in theory be integrated downward from the surface yielded estimates of the vertical velocity, w. The horizontal divergence was dominated by the meridional term, v_y, in most places. However, the shoaling of the EUC did result in a significant zonal term, u_x, in limited regions.

The largest feature in u_x (Fig. 6a) was the vertical dipole centered about the equator with zonal divergence above 105 m and convergence from 110 to 270 m. This pattern was due to the shoaling of the EUC. Equatorial zonal convergence below 270 m was the result of the growth of the westward-flowing EIC west of 140°W (Fig. 3a). Zonal convergence in the NECC and SEC was due to slight eastward weakening of the eastward-flowing NECC and slight westward strengthening of the westward flowing SEC, as expected from the Sverdrup balance. Zonal convergences centered near 230 m, $\pm 3°$ latitude were tightly linked to divergences 60–80 m shallower and about 2° poleward. This pattern was due to the shoaling and poleward shift of the NSCC and SSCC as they move eastward (Johnson and Moore 1997). A more local estimate of u_x from the slope of a third-order polynomial evaluated at 136°W significantly increased the magnitude of the dipole on the equator (Fig. 7a, dash–dotted line), and other features off the equator (not shown), but was not appropriate for a large-scale estimate of w.

Since $u \gg v$ and $v_y \gg u_x$, v_y (Fig. 6b) was contoured at five times coarser intervals than u_x. On the equator surface meridional divergence, v_y, was strong (Fig. 7b) at 60 (± 20) $\times 10^{-8}$ s^{-1}. Meridional convergence in the thermocline reached 30 (± 10) $\times 10^{-8}$ s^{-1} on the equator. The transition from meridional divergence to convergence occurred at 50 m. Near-surface meridional con-
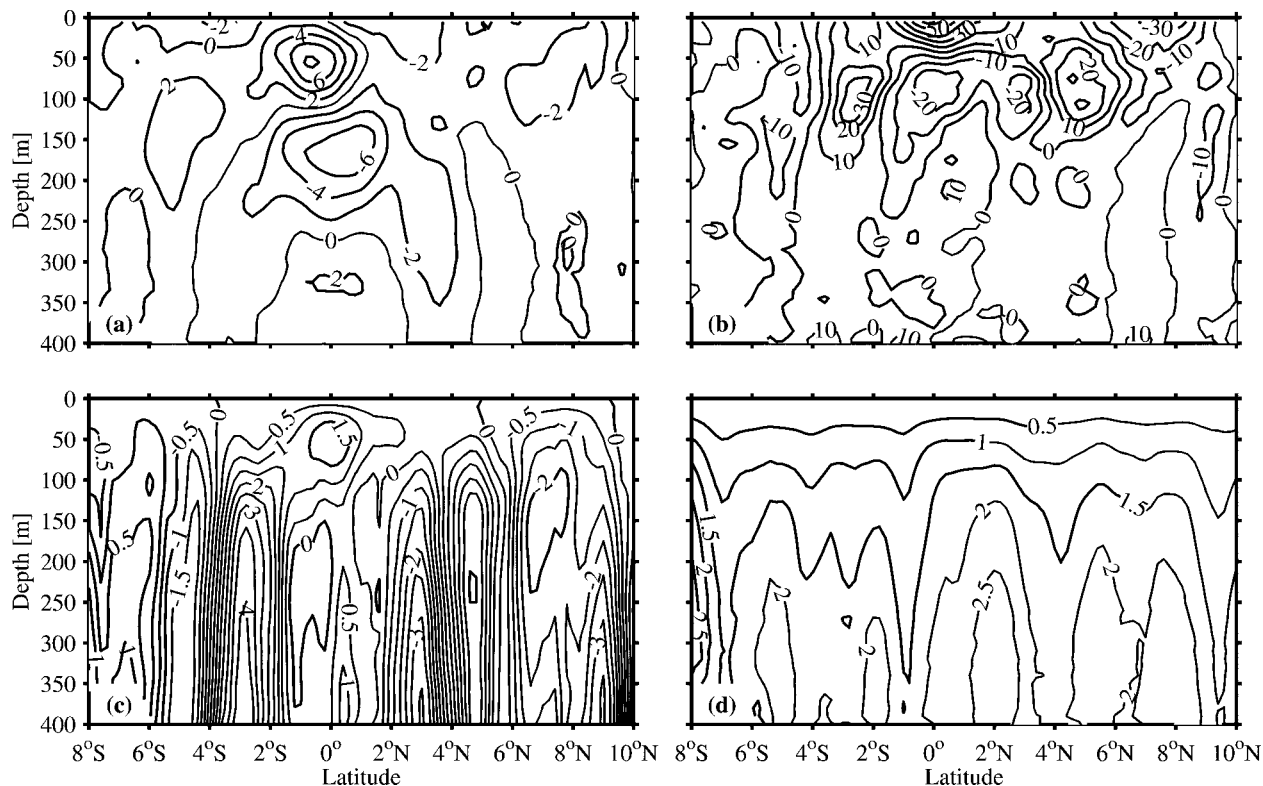
FIG. 6. Vertical–meridional sections based on data taken from 170°–95°W (see text). (a) Zonal divergence, u_x (10^{-8} s^{-1}) from linear fits of u vs longitude; contour intervals (CI) 2, positive shaded. (b) Meridional divergence, v_y (10^{-8} s^{-1}); CI 10, positive shaded, estimated as in Fig. 5. (c) Vertical velocity, w (10^{-5} m s^{-1}); CI 0.5, positive (upward) shaded. (d) Standard error of w, e_w (10^{-5} m s^{-1}); CI 0.5, $|w| > e_w$ shaded.

vergence was found from 5° to 9°N, coincident with the NECC. Finally, subsurface off-equatorial meridional divergence reached 40 ($\pm$10) $\times$ 10^{-8} s^{-1} near 115 m, 3°S and 30 ($\pm$10) $\times$ 10^{-8} s^{-1} near 105 m, 5°N, locations where the equatorward flow in the thermocline diminished toward the poles. Equatorward geostrophic ve-

locities (not shown) dropped off much more gradually than the directly measured ones, and thus suggested that the subsurface off-equatorial meridional divergences may have been overestimated and too localized.

The vertical velocity was estimated from these two fields by combining them to find the horizontal diver-
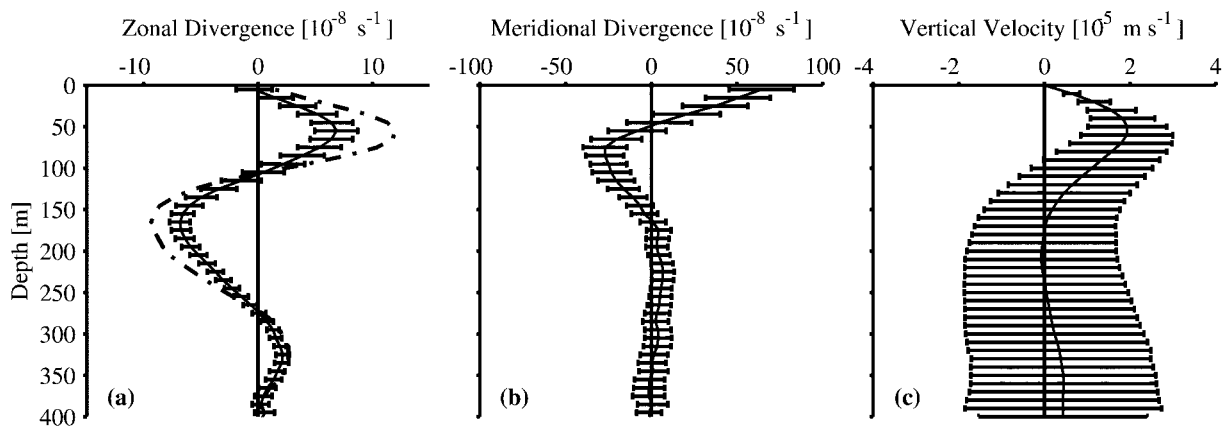

FIG. 7. Mean properties at the equator plotted with standard error bars against depth, based on data taken from 170° to 95°W (see text). (a) Zonal divergence, u_x (10^{-8} s^{-1}), from the slopes of linear (solid line with error bars) and third-order polynomial (dash–dot line) fits of u vs longitude. (b) Meridional divergence, v_y (10^{-8} s^{-1}), estimated as in Fig. 5. (c) Vertical velocity, w (10^{-5} m s^{-1}) is the downward vertical integral of the sum of panels a and b.

gence and then integrating down from the surface (Fig. 6c). Only the regions where w exceeded one standard error (shading in Fig. 6d) were considered possibly significant and worthy of discussion. Equatorial upwelling was found above the EUC core, with a value of 1.9 ($\pm$0.9) $\times$ 10^{-5} m s^{-1} at 50 m (Fig. 7c). Meridionally integrating w between 3.6°S and 5.2°N and applying the results to the sampled region of 170°–95°W resulted in net upwelling of 62 ($\pm$18) $\times$ 10^6 m^3 s^{-1} across 50 m, the most robust estimate from the upwelling calculation. Significant near-surface downwelling occurred within the NECC between 6° and 9°N (Figs. 6c and 6d). At 50 m, downwelling peaked at -1.5 ($\pm$0.8) $\times$ 10^{-5} m s^{-1} near 7.8°N. However, the apparent strong meridional convergence south of 10°N may have been exaggerated above 20 m because of previously mentioned problems extrapolating ADCP velocities to the surface around a shallow mixed layer and strong thermocline. Thus the strength of downwelling within the NECC may have been overestimated.

Interpretation of w below around 100 m was problematic, as vertical integration of noise in the horizontal divergence field started to dominate. By 200 m, w appeared to be composed of a series of very strong, fairly depth-independent upwellings and downwellings, changing sign roughly every 2° of latitude (Fig. 6c). Tellingly, the distance for sign changes was about the same size as the window used to estimate v_y. While these strong vertical velocities stood out from the standard error of the mean over nearly a third of the domain (Fig. 6d), this is just about the proportion expected for random noise. Finally, the subthermocline vertical velocities remained roughly constant from 200 m down to the bottom of the sampled region, 400 m. This behavior seems unlikely. For instance, the model of Marin et al. (2000) for the subsurface countercurrents (SCCs) predicts subthermocline downwelling on the equator and upwelling at the SCCs, but these model w exist in a limited region just below the thermocline, associated with the equatorial thermostad.

5. Discussion

The zonal currents reported in this study complement those of WK. The EUC transport here was larger than in WK and the EIC transport was smaller. These differences are consistent with zonal structure of the zonal velocity (Fig. 3a), which showed a stronger EUC and weaker EIC at 136°W than at 154°W. The NECC and total SEC transports reported here were smaller than in WK. These differences in off-equatorial current transports were in the correct sense for zonal differences predicted by the Sverdrup relation, which would have both of these current transports increasing in magnitude to the west. Of coarse, the choice of reference level and lack of ageostrophic velocities in the WK estimates could also account for some transport differences. Velocities used for this study were directly measured rather

than inferred from geostrophic calculations referenced to 1000 dbar as in WK. Direct velocity measurements around the equator have shown that 1000 dbar is not necessarily an entirely satisfactory level of no motion, even in the mean (Firing et al. 1998), and some near-surface ageostrophy is to be expected. Another big difference was the sparse sampling over an 8-yr period and a wide longitude range for this study compared with the well-sampled year and small longitude range in WK. Zonal currents tend to change position (depth and latitude) and strength (velocity and area) with changes in longitude, season, phase of the SOI, and under more transient influences. The simple polynomial fits versus longitude made here do not account for all of those variations. For instance, the NSCC and SSCC transports and velocities reported here were much weaker than those from analysis of the synoptic CTD/ADCP sections (Rowe et al. 2000). Those eastward currents vary in latitude over time and are embedded in westward flow, so simple Eulerian averaging schemes such as those in this study reduce their magnitude.

The direct, large-scale estimate of equatorial upwelling transport reported here, 62 ($\pm$18) m^3 s^{-1} across 50 m, in the area bounded by 3.6°S–5.2°N, 170°W–95°W, is slightly higher than, but agrees within error bars with previous indirect large-scale estimates (all between 5°S and 5°N), but only when the estimates are scaled by the zonal distances over which they were made. One estimate from the oceanic ^{14}C distribution was 39 ($\pm$11) $\times$ 10^6 m^3 s^{-1} across 50 m between 170° and 90°W (Quay et al. 1983). A simple box model based on geostrophy, Ekman dynamics, and mass and heat budgets between 170°E and 100°W gave an upwelling of 50 $\times$ 10^6 m^3 s^{-1} across 50 m (Wyrtki 1981). A similar but more detailed diagnostic model yielded an estimate of 22 $\times$ 10^6 m^3 s^{-1} across 62.5 m (Bryden and Brady 1985). This estimate was made between 150° and 110°W, so, while it is nearly three times smaller than that presented here, it covers little more than half the longitudinal range.

The upwelling velocity reported here, 1.9 ($\pm$0.9) $\times$ 10^{-5} m s^{-1} at 50 m, was larger than estimated by Wyrtki, 1.15 $\times$ 10^{-5} m s^{-1}, but smaller than that of Bryden and Brady, 2.9 $\times$ 10^{-5} m s^{-1}. These differences arise because Wyrtki assumed upwelling within 200 km of the equator, whereas Bryden and Brady confined it to within 83 km. The intermediate upwelling velocity found here, with a meridional decay scale near 175 km, was determined directly, although probably broadened by the smoothing from the objective mapping and estimation of v_y over 2° latitude. Drifter data analysis (Poulain 1993) suggests that equatorial upwelling may be more meridionally localized than the resolution of this study, hence stronger. However, the equatorial upwelling transport estimated here was not likely to have been influenced by this potential resolution problem because it was made over a latitude range much greater than the meridional smoothing scales employed.

The large-scale equatorial upwelling velocity estimated here from shipboard CTD/ADCP sections was somewhat larger than, but again agreed within error bars with, a local estimate from a current meter array around the equator and 140°W (WQ). However, there are a few obvious differences. First, the zonal divergence on the equator reported here (Figs. 6a and 7a) was somewhat less than that of WQ. This difference was probably due to the much larger zonal extent (75° vs 4°) over which the zonal gradients were estimated here compared to in WQ. A more local estimate of equatorial zonal divergence near 136°W (Fig. 7a, dash–dot line) was in better agreement with the WQ estimate. Second, the error estimates for vertical velocity here (Fig. 3f) were much larger than those of WQ, probably due to the differences between estimating horizontal divergence over a very large area using sporadic snapshots of current, temperature, and salinity over 8.5 years versus doing so over smaller spatial scales with a time series from May 1990 through June 1991. Third, WQ reported significant near-equatorial downwelling below the thermocline, which was not seen here. However, the error bars for w were so large here below 100 m on the equator as to rule out comment on even the sign of w below the thermocline (Figs. 6d and 7c).

Off the equator, the estimates of w made here showed a large and significant near-surface downwelling in the NECC (Figs. 6c and 6d), as has been anticipated by latitudinal wind stress and thermocline depth variations (WK). This pattern also emerged from a very similar calculation using a smaller, independent ADCP dataset (Johnson and Luther 1994). In addition, the meridional convergence forcing this downwelling is evident, although slightly weaker than here, in surface drifter data (Baturin and Niiler 1987).

The temperatures of the surface divergence and the subsurface convergence are of interest as an indication of the depth from which the equatorial upwelling was fed. The poleward surface transports started at 25.5°C near the equator and warmed to about 27.5°C by ±8°. On the other hand, the mean temperatures of the equatorward thermocline transports were about 20.5°C in the Southern Hemisphere and 23°C in the Northern Hemisphere. The dominance of the Southern Hemisphere in the thermocline convergence implied a mean temperature difference between source water and upwelled water on the equator of about 4°C. This difference was the same as that suggested for an earlier budget (Wyrtki 1981) in which the surface heating was also included. Also, equatorward thermocline velocities reached to temperatures at as low as 13°C (about $\sigma_\theta = 26.4$ kg m^{-3}) in the south and 16°C (about 25.7 kg m^{-3}) in the north, somewhat lighter and shallower than the lower bound of 26.5 kg m^{-3} from chemical tracers (Fine et al. 1983; Quay et al. 1983).

The most unusual aspect of this study lies in direct measurements of the subsurface meridional flow field, which have rarely been reported (but see Johnson and

Luther 1994). An intriguing feature of the meridional velocity was greater poleward surface flow in the north combined with greater equatorward thermocline flow in the south. This asymmetry in the convergence and divergence tended to bring in more Southern Hemisphere water at depth and remove more surface water to the north in the amount of roughly 10×10^6 m^3 s^{-1}. Applied over the entire longitude range of the survey, the near-surface poleward transport at 5°N was 34 (±17) $\times$ 10^6 m^3 s^{-1} compared with -23 (±9) $\times$ 10^6 m^3 s^{-1} at 5°S. The asymmetry in poleward near-surface flow has been observed in earlier shipboard ADCP data (Johnson and Luther 1994) and drifter data (Baturin and Niiler 1997). In the thermocline, equatorward transports peaked at 30 (±17) $\times$ 10^6 m^3 s^{-1} at 1.6°S and -20 (±21) $\times$ 10^6 m^3 s^{-1} at 3.6°N. Interior thermocline convergence on the equator has also been estimated to be roughly 10×10^6 m^3 s^{-1} greater in the Southern Hemisphere than the Northern Hemisphere using geostrophy at slightly higher latitudes (Johnson and McPhaden 1999). Of course the error bars on the direct velocity estimates are so large as to make this agreement quite likely fortuitous.

The possible presence of stronger poleward surface flow in the north was initially puzzling, as the trade winds were stronger in the south than in the north. However, the strong surface meridional shears in the NECC and the SEC reduced the effective Coriolis parameter north of the equator (to as little as 75% of nominal at 3°N) and increased it south of the equator (to as much as 110% of nominal at 2.5°S), allowing slightly stronger Ekman transport in the north than in the south despite the winds, localized to within 100 km of ±3° latitude. In addition, the opposition of the NECC to the winds imparted a greater effective stress north of 5°N, raising the northward Ekman transport there, while the SEC running with the winds slightly reduced the effective stress to the south (Kelly et al. 2000). Finally, equatorward surface geostrophic flows were also about 0.02 m s^{-1} larger in the south than in the north, acting to reduce the poleward surface Ekman flow in the south more than in the north. These three effects may have combined to resolve the discrepancy between observed meridional flows and those expected from zonal wind stresses, certainly within the errors.

At any rate, the observed 10×10^6 m^3 s^{-1} asymmetries in meridional flow, while highly uncertain, could constitute a possible mechanism for interhemispheric exchange, where thermocline water primarily from the Southern Hemisphere is upwelled at the equator, with some combination of mixing and surface forcing erasing its negative potential vorticity, and then carried north at the surface. This process is found in numerical models (Blanke and Raynaud 1997; Lu et al. 1998; Rodgers et al. 1999). However, a more detailed and better constrained evaluation of the 3D flow field in the equatorial Pacific will be required to fully evaluate this possible interhemispheric pathway using observations. Some such mechanism for interhemispheric trans-

port is ultimately required to supply the Indonesian Throughflow. The throughflow has a transport (Gordon et al. 1999) of a similar order to the observed asymmetry, and is fed by waters that have been cycled through the North Pacific (Ffield and Gordon 1992) as part of the global thermohaline circulation. A similar conversion of intermediate water to surface water takes place in the equatorial Atlantic (Roemmich 1983), where a net northward flow of warm water is required to balance southward export of North Atlantic Deep Water, another component of the global thermohaline circulation.

REFERENCES

Baturin, N. G., and P. P. Niiler, 1997: Effects of instability waves in the mixed layer of the equatorial Pacific. *J. Geophys. Res.,* **102,** 27 771–27 793.

Blanke, B., and S. Raynaud, 1997: Kinematics of the Equatorial Undercurrent: An Eulerian and Lagrangian approach from GCM results. *J. Phys. Oceanogr.,* **27,** 1038–1053.

Bryden, H. L., and E. C. Brady, 1985: Diagnostic model of the three-dimensional circulation in the upper equatorial Pacific Ocean. *J. Phys. Oceanogr.,* **15,** 1255–1273.

Chavez, F. P., P. G. Strutton, G. E. Friederich, R. A. Feely, G. Feldman, D. Foley, and M. J. McPhaden, 1999: Biological and chemical response of the equatorial Pacific Ocean to the 1997–1998 El Niño. *Science,* **286,** 2126–2131.

Chelton, D. B., F. J. Wentz, C. L. Gentemann, R. A. de Szoeke, and M. G. Schlax, 2000: Satellite microwave SST observations of transequatorial tropical instability waves. *Geophys. Res. Lett.,* **27,** 1239–1242.

Efron, B., 1982: *The Jackknife, the Bootstrap, and Other Resampling Plans.* CBMS-NSF Regional Conference Series in Applied Mathematics, Vol. 38, SIAM, 92 pp.

Ffield, A., and A. L. Gordon, 1992: Vertical mixing in the Indonesian thermocline. *J. Phys. Oceanogr.,* **22,** 184–195.

Fine, R. A., W. G. Peterson, C. G. H. Rooth, and H. G. Östlund, 1983: Cross-equatorial tracer transport in the upper waters of the Pacific Ocean. *J. Geophys. Res.,* **88,** 763–769.

Firing, E., S. E. Wijffels, and P. Hacker, 1998: Equatorial subthermocline currents across the Pacific. *J. Geophys. Res.,* **103,** 21 413–21 423.

Flament, P., S. Kennan, R. Knox, P. Niiler, and R. Bernstein, 1996: The three-dimensional structure of a tropical instability wave. *Nature,* **383,** 610–613.

Gordon, A. L., R. D. Susanto, and A. L. Ffield, 1999: Throughflow within Makassar Strait. *Geophys. Res. Lett.,* **26,** 3325–3328.

Halpern, D., R. A. Knox, D. S. Luther, and S. G. H. Philander, 1989: Estimates of equatorial upwelling between 140° and 110°W during 1984. *J. Geophys. Res.,* **94,** 8018–8020.

Hellerman, S., and M. Rosenstein, 1983: Normal monthly wind stress over the world ocean with error estimates. *J. Phys. Oceanogr.,* **13,** 1093–1104.

Johnson, E. S., and D. S. Luther, 1994: Mean zonal momentum balance in the upper and central equatorial Pacific Ocean. *J. Geophys. Res.,* **99,** 7689–7705.

——, and P. E. Plimpton, 1999: TOGA/TAO shipboard ADCP data report, 1991–1995. NOAA Data Rep. ERL PMEL-67, 23 pp.

Johnson, G. C., and D. W. Moore, 1997: The Pacific subsurface countercurrents and an inertial model. *J. Phys. Oceanogr.,* **27,** 2448–2459.

——, and M. J. McPhaden, 1999: Interior pycnocline flow from the subtropical to the equatorial Pacific Ocean. *J. Phys. Oceanogr.,* **29,** 3073–3098.

——, ——, G. D. Rowe, and K. E. McTaggart, 2000: Upper equatorial Pacific Ocean current and salinity variability during the 1996–1998 El Niño–La Niña cycle. *J. Geophys. Res.,* **105,** 1037–1053.

Kelly, K. A., S. Dickinson, and G. C. Johnson, 2000: The effect of ocean currents on the winds measured by scatterometers. *Eos, Trans. Amer. Geophys. Union,* **81** (22), (Suppl.), WP74.

Lu, P., J. P. McCreary Jr., and B. A. Klinger, 1998: Meridional circulation cells and the source waters of the Pacific Equatorial Undercurrent. *J. Phys. Oceanogr.,* **28,** 62–84.

Marin, F., B. L. Hua, and S. Wacogne, 2000: The equatorial thermostad and subsurface countercurrents in light of the dynamics of atmospheric Hadley cells. *J. Mar. Res.,* **58,** 405–437.

Murray, J. W., E. Johnson, and C. Garside, 1995: A U.S. JGOFS process study in the equatorial Pacific (EqPac): Introduction. *Deep-Sea Res. Part II,* **42,** 275–293.

Philander, S. G. H., 1990: *El Niño, La Niña, and the Southern Oscillation.* Academic Press 289 pp.

Poulain, P.-M., 1993: Estimates of horizontal divergence and vertical velocity in the equatorial Pacific. *J. Phys. Oceanogr.,* **23,** 601–607.

Quay, P. D., M. Stuiver, and W. S. Broecker, 1983: Upwelling rates for the equatorial Pacific Ocean derived from the bomb 14C distribution. *J. Mar. Res.,* **41,** 769–792.

Rodgers, K. B., M. A. Cane, N. H. Naik, and D. P. Schrag, 1999: The role of the Indonesian throughflow in equatorial Pacific thermocline ventilation. *J. Geophys. Res.,* **104,** 20 551–20 570.

Roemmich, D., 1983: The balance of geostrophic and Ekman transports in the tropical Atlantic Ocean. *J. Phys. Oceanogr.,* **13,** 1534–1539.

Rowe, G. D., E. Firing, and G. C. Johnson, 2000: Pacific Equatorial Subsurface Countercurrent velocity, transport, and potential vorticity. *J. Phys. Oceanogr.,* **30,** 1172–1187.

Stricherz, J., J. J. O'Brien, and D. M. Legler. 1992: *Atlas of Florida State University Tropical Pacific Winds for TOGA, 1966–1985.* The Florida State University, 275 pp.

Taft, B. A., and W. S. Kessler, 1991: Variations of zonal currents in the central tropical Pacific during 1970 to 1987: Sea level and dynamic height measurements. *J. Geophys. Res.,* **96,** 12 599–12 618.

Wang, W., and M. J. McPhaden, 1999: The surface-layer heat balance in the Equatorial Pacific Ocean. Part I: Mean seasonal cycle. *J. Phys. Oceanogr.,* **29,** 1812–1831.

Weisberg, R. H., and L. Qiao, 2000: Equatorial upwelling in the central Pacific estimated from moored velocity profilers. *J. Phys. Oceanogr.,* **30,** 105–124.

Wyrtki, K., 1981: An estimate of equatorial upwelling in the Pacific. *J. Phys. Oceanogr.,* **11,** 1205–1214.

——, and B. Kilonsky, 1984: Mean water and current structure during the Hawaii-to-Tahiti shuttle experiment. *J. Phys. Oceanogr.,* **14,** 242–254.

Yu, X., and M. J. McPhaden, 1999: Seasonal variability in the equatorial Pacific. *J. Phys. Oceanogr.,* **29,** 925–947.

CORRIGENDUM

In the article ''Equatorial Pacific Ocean horizontal velocity, divergence, and upwelling,'' which appeared in the March 2001 *Journal of Physical Oceanography*, Vol. **31,** No. 3, 839–849, part of the shaded regions in panels (c) and (d) of Fig. 6 on page 846. The missing shading describes the author's major finding of significant upwelling on the equator, does not appear in the illustrations due to a production difficulty. The correct figure, showing the shaded regions from about 4°S to 6°N and at 10°N in panel (c) and from about 4°S to 2°N and 6°N to 9°N in panel (d) that are missing in the illustration printed in the March issue, is printed below.
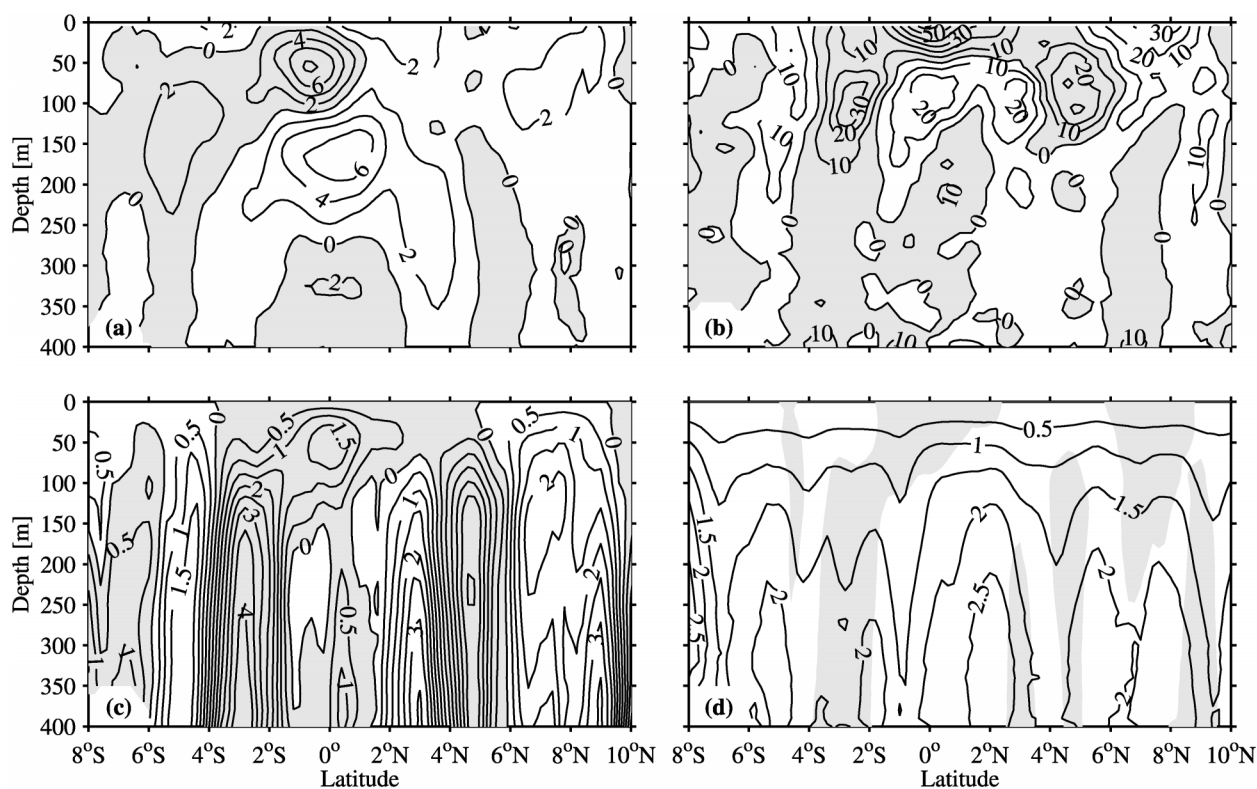

FIG. 6. Vertical–meridional sections based on data taken from 170°–95°W (see text). (a) Zonal divergence, u_x ($10^{-8}s^{-1}$) from linear fits of u vs longitude; contour intervals (CI) 2, positive shaded. (b) Meridional divergence, v_y ($10^{-8}s^{-1}$); CI 10, positive shaded, estimated as in Fig. 5. (c) Vertical velocity, w ($10^{-5}s^{-1}$); CI 0.5, positive (upward) shaded. (d) Standard error of w, e_w ($10^{-5}s^{-1}$); CI 0.5, $|w| > e_w$ shaded.